Coulomb correction effect in Delbrück scattering and atomic Rayleigh scattering of 1–4 MeV photons

B. Kasten, D. Schaupp,* P. Rullhusen, F. Smend, and M. Schumacher
II. Physikalisches Institut der Universität Göttingen, D-3400 Göttingen, Federal Republic of Germany

Lynn Kissel
Sandia National Laboratories, Albuquerque, New Mexico 87185
(Received 22 October 1985)

Previous large-angle investigations of atomic Rayleigh and Delbrück scattering in the few MeV energy range have been extended to small scattering angles. Rayleigh predictions obtained by combining the second-order S matrix for inner shells with the modified form factor for outer shells are accurate to better than 3%. Tentative estimates of Coulomb correction terms for the Delbrück amplitudes are obtained from the experimental differential cross sections using (i) general properties of scattering amplitudes, (ii) information from pair production valid at small angles, and (iii) rather firm arguments concerning signs and relative magnitudes of the scattering amplitudes at large angles and assumptions about the relative magnitudes of the Coulomb correction amplitudes at intermediate energies.

I. INTRODUCTION

Low-energy elastic photon scattering is known to be a coherent superposition of atomic Rayleigh (R), nuclear Thomson (T), nuclear Rayleigh (N), and Delbrück (D) scattering. Of these components, R and N scattering proceed through the virtual excitation of the atomic cloud and the nuclear giant-dipole resonance (GDR), respectively. Low-energy T scattering may simply be understood as a center of mass motion of the nucleus. D scattering is a consequence of the polarization of the vacuum. Predictions are easily obtained for the nuclear scattering amplitudes T and N, whereas calculations of R and D require quantum electrodynamical procedures which have become tractable only in the last 10 years.

Previous systematic investigations of R and D scattering, both experimental and theoretical, carried out mostly at large angles, have led to the following insights[1–6] into properties of these components. Below 0.8 MeV elastic photon scattering is only due to R and T scattering. The agreement achieved between theory and experiment is on a few percent level. For uranium ($Z=92$) as the scattering material, D scattering has been observed[7–9] at energies as low as 0.9 MeV, i.e., below the pair production threshold, and was found to be in agreement with the lowest-order prediction up to about 2 MeV. At 2.75 MeV and higher energies, large modifications of D scattering due to the Coulomb correction effect have been found.[10] The Coulomb correction term has been shown to be of the order $\alpha(Z\alpha)^4$ with no significant[1] contribution of higher orders in Z. Below $Z=50$, where Coulomb corrections are small, the predicted lowest-order amplitudes have been tested and found valid[11] within 5%. In the 8–12 MeV energy range elastic scattering mainly proceeds through the excitation of the GDR. By a systematic study of the energy and Z dependence of elastic scattering it was possible to simultaneously improve on the GDR parameters and to arrive at quantitative results for the Coulomb correction terms.[12] Though assumptions had to be made in order to reduce the number of adjustable parameters, the empirical Coulomb correction terms have proved to be very helpful in clarifying the properties of D scattering.

One aim of the present investigation was to improve on our knowledge of R scattering in the MeV energy and forward angular range, where firm information is very scarce. For this purpose (i) L_I shell R amplitudes have been calculated at 2.754 MeV from the second-order S matrix, where previously only form factor estimates were available, (ii) S matrix R calculations for the K shell have been extended from the previous limit of 2.754 to 4.8 MeV, and (iii) elastic differential cross sections have been measured at small scattering angles of 7.7° and 15°. Another aim was to obtain quantitative results for the Coulomb correction term in D scattering in the energy range around 3 MeV, where a very clear-cut investigation is possible because contributions of N scattering are not of importance. For this purpose previous elastic differential cross section measurements with 2.754 MeV photons were extended to smaller angles and a systematic analysis of the Z dependence of elastic scattering between 0° and 150° has been carried out. This study makes use of available knowledge on Coulomb and screening corrections at $\theta=0°$ obtained from the pair production cross section.[13,14] With the data we are presenting we hope to stimulate an exact calculation of the Coulomb correction effect, which certainly is very difficult to perform.

II. EXPERIMENT

For the present experiments carried out at scattering angles of 30° and 45° the same geometry and the same rectangular scatterers were used as in previous experiments[11] at larger angles. For the smaller angles of $\theta=15°$ and 7.7° sizable uncertainties due to the angular divergence were

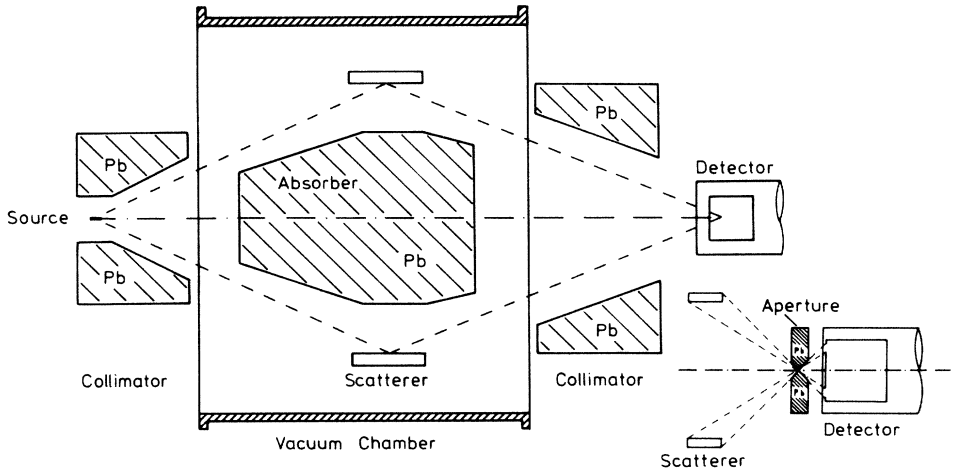

FIG. 1. Experimental arrangement (not to scale) used for small-angle scattering experiments. With the aperture shown in the inset the angular divergence was $\Delta\theta=0.7°$. Distance between source and detector: $d=181$ cm for $\theta=7.7°$ and $d=157$ cm for $\theta=15°$. The scatterers were cylindrical rings with diameters of 6.1 cm (9.3 cm) and a length of 2.0 cm (7.7 cm) for the scattering angle 7.7° (15°).

expected when using this geometry. Therefore, the ring geometry of Fig. 1 was adopted which allows one to largely reduce the angular divergence without loss in count rate. The source used for the $\theta=15°$ and 7.7° experiments consisted of about 20 mCi of ^{56}Co and was prepared by bombarding a 2 mm$\times$20 mm cylinder of Fe in the internal beam of the Göttingen cyclotron. For a scattering angle of $\theta=15°$ the full Ge(Li) detector was exposed to the scattered radiation (upper part of Fig. 1), whereas for $\theta=7.7°$ an aperture was placed in front of the detector (inset of Fig. 1) in a way that radiation passing through the aperture was absorbed in the active zone of the true coaxial Ge(Li) detector. With the latter geometry the angular divergence was $\Delta\theta=0.7°$. The solid angle has been calculated taking into account the angular-dependent efficiency of the Ge(Li) detector with and without the aperture in front of it. This efficiency was measured with a point source of ^{56}Co at different positions at the place of the scatterer. Also, the angular distribution of gamma rays emitted from the source was carefully measured and taken into account.

As an example Fig. 2 shows the spectrum of scattered photons obtained at $\theta=15°$ using a Pb scatterer. In this spectrum the room background was eliminated by sub-

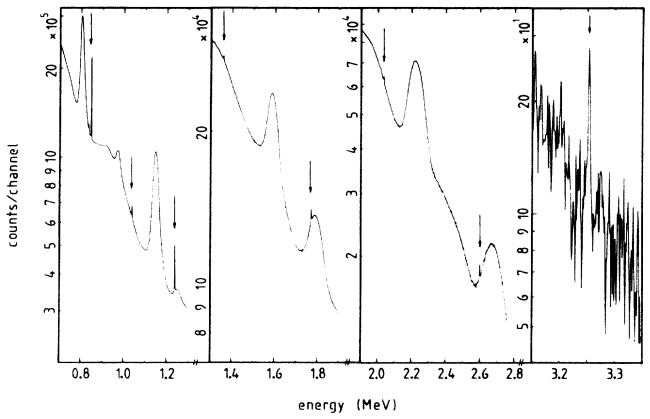

FIG. 2. Spectrum of photons scattered by lead through a scattering angle of $\theta=15°$. Lines indicated by arrows are full-energy peaks of elastically scattered photons. Broad peaks are profiles of Compton scattered photons.

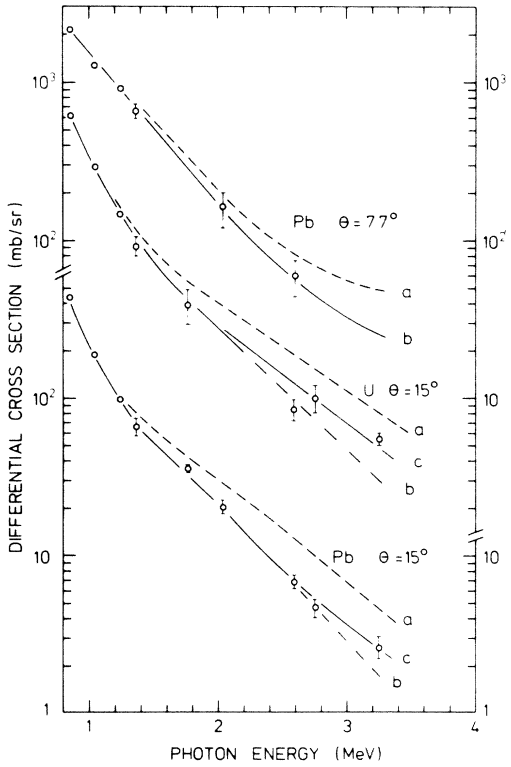

FIG. 3. Experimental small-angle elastic scattering cross sections compared with different predictions: (a) including R, T, and N scattering only, (b) including R, T, N, and lowest-order D scattering but not including the Coulomb correction term, (c) same as (b) but including also the Coulomb correction term.

TABLE I. Experimental elastic differential cross sections for the scattering of photons from Pb through $\theta=7.7°$ compared with different predictions. MFF: including lowest-order D scattering and R scattering as given by the modified form factor (MFF). SM: including lowest-order D scattering and R scattering as given by the second-order S matrix (SM). WD: without D scattering but with R scattering as given by the SM. Errors are given in parentheses.

E_γ (keV)	$(d\sigma/d\Omega)_{\mathrm{MFF}}$ (mb/sr)	$(d\sigma/d\Omega)_{\mathrm{SM}}$ (mb/sr)	$(d\sigma/d\Omega)_{\mathrm{WD}}$ (mb/sr)	$(d\sigma/d\Omega)_{\mathrm{expt}}$ (mb/sr)
847	2093	2093	2120	2105(60)
1038	1319	1319	1349	1257(40)
1238	910	913	946	919(20)
1360	712.7	712.3	746.3	662(80)
2035	149.5	151.4	184.4	163(43)
2598	55.1	54.2	82.3	60(16)

TABLE II. Elastic differential cross sections for the scattering of photons from U through $\theta=15°$. The notations are the same as in Table I.

E_γ (keV)	$(d\sigma/d\Omega)_{\mathrm{MFF}}$ (mb/sr)	$(d\sigma/d\Omega)_{\mathrm{SM}}$ (mb/sr)	$(d\sigma/d\Omega)_{\mathrm{WD}}$ (mb/sr)	$(d\sigma/d\Omega)_{\mathrm{expt}}$ (mb/sr)
847	601.5	600.1	614.4	612(13)
1038	297.9	297.1	308.4	291.9(8.8)
1238	146.6	149.8	162.8	146.6(3.3)
1360	101.7	101.7	114.5	92.1(13.3)
1771	42.4	41.4	54.0	39.3(9.9)
2598	11.3	9.9	18.8	8.4(1.4)
3253	3.46	3.06	8.09	5.5(0.4)[a]

[a]Corrected for nuclear resonance fluorescence (NRF) using (Ref. 18) $\sigma_{\mathrm{NRF}}=7.4\pm0.1$ mb.

TABLE III. Elastic differential cross sections for the scattering of photons from Pb through $\theta=15°$. The notations are the same as in Table I.

E_γ (keV)	$(d\sigma/d\Omega)_{\mathrm{MFF}}$ (mb/sr)	$(d\sigma/d\Omega)_{\mathrm{SM}}$ (mb/sr)	$(d\sigma/d\Omega)_{\mathrm{WD}}$ (mb/sr)	$(d\sigma/d\Omega)_{\mathrm{expt}}$ (mb/sr)
847	402.1	410.1	417.3	435.2(9.8)
1038	183.4	190.5	195.7	188.7(6.1)
1238	96.1	97.4	105.7	98.9(2.4)
1360	71.6	69.8	78.3	65.7(9.0)
1771	34.4	33.0	41.9	35.7(2.2)
2035	22.0	20.4	28.9	20.4(2.2)
2598	7.7	6.8	12.8	6.9(0.7)
3253	1.88	1.70	4.68	2.6(0.4)

TABLE IV. Scattering amplitudes and differential cross sections for elastic scattering of 2.754 MeV photons. Each entry in the third through seventh columns gives, in two lines, the amplitudes for || and ⊥ polarization, respectively. A_R, atomic Rayleigh; A_D lowest-order Delbrück; B_D, Coulomb correction term of D amplitude; A_T, nuclear Thomson; A_N, nuclear Rayleigh. $(d\sigma/d\Omega)_{\rm LO}$ includes all amplitudes without the Coulomb correction term, $d\sigma/d\Omega$ includes also the Coulomb correction term, $(d\sigma/d\Omega)_{\rm expt}$ is the experimental result with error parentheses.

θ (deg)	Z	$A_{R\perp}^{\parallel}$ ($10^{-3}\ r_0$)	$A_{D\perp}^{\parallel}$ ($10^{-3}\ r_0$)	$B_{D\perp}^{\parallel}$ ($10^{-3}\ r_0$)	$A_{T\perp}^{\parallel}$ ($10^{-3}\ r_0$)	$A_{N\perp}^{\parallel}$ ($10^{-3}\ r_0$)	$d\sigma/d\Omega_{\rm LO}$ (μb/sr)	$d\sigma/d\Omega$ (μb/sr)	$d\sigma/d\Omega_{\rm expt}$ (μb/sr)
30	92	$-38.74+4.992i$	$78.87+44.67i$	$-13.32+24.36i$	-16.88	1.643	233.2	394.6	389(40)
		$-61.12+18.00i$	$42.37+20.28i$	$-7.157+11.06i$	-19.49	1.898			
	82	$-20.91+3.626i$	$62.66+35.48i$	$-8.409+15.37i$	-15.35	1.406	132.7	198.0	216(17)
		$-34.93+11.02i$	$33.66+16.11i$	$-4.517+6.980i$	-17.72	1.624			
	73	$-9.760+2.470i$	$49.66+28.12i$	$-5.282+9.655i$	-14.00	0.9493	82.72	109.1	92.5(8.7)
		$-18.52+6.697i$	$26.67+12.77i$	$-2.837+4.384i$	-16.17	1.096			
	58	$-1.543+1.006i$	$31.35+17.75i$	$-2.105+3.848i$	-11.41	0.7065	32.83	37.80	33.9(5.0)
		$-4.901+2.430i$	$16.84+8.061i$	$-1.131+1.747i$	-13.18	0.8158			
	50	$-0.0142+0.5305i$	$23.30+13.19i$	$-1.162+2.125i$	-10.24	0.5498	16.90	18.82	18.6(2.2)
		$-1.810+1.239i$	$12.51+5.991i$	$-0.6244+0.9649i$	-11.82	0.6348			
45	92	$3.206+4.253i$	$45.07+25.69i$	$-5.373+15.76i$	-13.78	1.342	109.1	149.4	132(11)
		$-12.71+14.44i$	$16.23+4.778i$	$-1.934+2.931i$	-19.49	1.898			
	82	$4.258+3.060i$	$35.81+20.41i$	$-3.391+9.947i$	-12.53	1.148	63.31	81.32	83.9(4.0)
		$-4.848+8.702i$	$12.89+3.795i$	$-1.221+1.850i$	-17.72	1.624			
	73	$4.348+2.010i$	$28.38+16.18i$	$-2.130+6.248i$	-11.43	0.7751	36.45	44.66	43.7(2.6)
		$-0.9495+5.164i$	$10.22+3.008i$	$-0.7668+1.162i$	-16.17	1.096			
	58	$2.827+0.7873i$	$17.91+10.21i$	$-0.8487+2.490i$	-9.320	0.5769	12.03	13.94	15.4(2.1)
		$0.9853+1.821i$	$6.449+1.899i$	$-0.3055+0.4630i$	-13.18	0.8158			
	50	$1.924+0.4068i$	$13.31+7.588i$	$-0.4687+1.375i$	-8.358	0.4489	6.048	6.855	7.7(2.0)
		$0.9789+0.9137i$	$4.793+1.411i$	$-0.1687+0.2557i$	-11.82	0.6348			
60	92	$5.956+2.570i$	$29.43+16.65i$	$-0.7164+10.75i$	-9.745	0.9488	59.82	79.16	75.0(7.0)
		$-6.053+10.90i$	$5.589-0.6986i$	$-0.1360-0.4508i$	-19.49	1.898			
	82	$4.760+1.941i$	$23.38+13.23i$	$-0.4521+6.782i$	-8.860	0.8120	33.73	42.98	40.9(2.0)
		$-1.779+6.486i$	$4.440-0.5550i$	$-0.0859-0.2845i$	-17.72	1.624			
	73	$3.738+1.288i$	$18.53+10.49i$	$-0.2840+4.260i$	-8.088	0.5481	19.80	24.18	24.2(1.3)
		$0.0718+3.791i$	$3.519-0.4398i$	$-0.0539-0.1787i$	-16.17	1.096			
	58	$2.022+0.5111i$	$11.70+6.619i$	$-0.1132+1.697i$	-6.590	0.4079	7.780	8.798	10.00(1.0)
		$0.8040+1.312i$	$2.221-0.2777i$	$-0.0215-0.0712i$	-13.18	0.8158			
	50	$1.302+2.644i$	$8.693+4.919i$	$-0.0625+0.9375i$	-5.910	0.3174	4.951	5.357	5.47(0.18)
		$0.6884+0.6516i$	$1.651-0.2063i$	$-0.0119-0.0393i$	-11.82	0.6348			
75	92	$4.666+0.9181i$	$20.78+11.83i$	$1.755+7.164i$	-5.044	0.4911	44.41	56.07	52.0(6.0)
		$-4.935+8.181i$	$0.3516-2.912i$	$0.0297-1.763i$	-19.49	1.898			
	82	$3.401+0.9003i$	$16.51+9.399i$	$1.085+4.521i$	-4.586	0.4203	26.42	32.14	33.4(2.0)
		$-1.658+4.820i$	$0.2793-2.313i$	$0.0184-1.113i$	-17.72	1.624			
	73	$2.481+0.6576i$	$13.08+7.449i$	$0.6816+2.840i$	-4.185	0.2837	17.15	19.90	20.4(1.0)
		$-0.2938+2.786i$	$0.2213-1.833i$	$0.0115-0.6989i$	-16.17	1.096			
	58	$1.287+0.2855i$	$8.258+4.702i$	$0.2716+1.132i$	-3.411	0.2111	8.153	8.795	9.18(0.27)
		$0.3853+0.9495i$	$0.1397-1.157i$	$0.0046-0.2785i$	-13.18	0.8158			
	50	$0.8172+0.1517i$	$6.137+3.495i$	$0.1500+0.6250i$	-3.059	0.1643	5.747	5.996	5.78(0.13)
		$0.3661+0.4675i$	$0.1038-0.8600i$	$0.0025-0.1538i$	-11.82	0.6348			
90	92	$3.533-0.3924i$	$15.59+9.014i$	$2.149+4.298i$	0	0	41.81	49.42	47.6(3.1)
		$-4.478+6.278i$	$-2.569-3.899i$	$-0.3541-1.859i$	-19.49	1.898			
	82	$2.414+0.0893i$	$12.39+7.161i$	$1.356+2.713i$	0	0	26.47	30.35	31.0(1.6)
		$-1.730+3.654i$	$-2.041-3.097i$	$-0.2234-1.173i$	-17.72	1.624			
	73	$1.668+0.1769i$	$9.819+5.675i$	$0.9229+1.704i$	0	0	18.44	20.47	19.2(0.6)
		$-0.5722+2.085i$	$-1.618-2.455i$	$-0.1520-0.7369i$	-16.17	1.096			
	58	$0.8296+0.1182i$	$6.198+3.583i$	$0.3395+0.6790i$	0	0	9.530	10.02	10.57(0.33)
		$0.1110+0.6980i$	$-1.021-1.550i$	$-0.0559-0.2937i$	-13.18	0.8158			
	50	$0.5222+0.0693i$	$4.606+2.663i$	$0.1875+0.3750i$	0	0	6.877	7.082	6.62(0.15)
		$0.1635+0.3403i$	$-0.7588-1.152i$	$-0.0309-0.1622i$	-11.82	0.6348			

TABLE IV. (*Continued*).

θ (deg)	Z	$A_{R_\perp^\parallel}$ (10^{-3} r_0)	$A_{D_\perp^\parallel}$ (10^{-3} r_0)	$B_{D_\perp^\parallel}$ (10^{-3} r_0)	$A_{T_\perp^\parallel}$ (10^{-3} r_0)	$A_{N_\perp^\parallel}$ (10^{-3} r_0)	$d\sigma/d\Omega_{\rm LO}$ (μb/sr)	$d\sigma/d\Omega$ (μb/sr)	$d\sigma/d\Omega_{\rm expt}$ (μb/sr)
120	92	$2.645-2.047i$	$9.920+6.175i$	$1.433+1.791i$	9.745	−0.9488	46.99	52.02	50.51(4.1)
		$-3.601+4.150i$	$-5.454-4.566i$	$-0.7877-1.324i$	−19.49	1.898			
	82	$1.543-0.9368i$	$7.881+4.905i$	$0.9042+1.130i$	8.860	−0.8120	32.08	34.77	34.7(1.6)
		$-1.600+2.316i$	$-4.332-3.627i$	$-0.4971-0.8358i$	−17.72	1.624			
	73	$0.9289-0.4271i$	$6.246+3.888i$	$0.5680+0.7100i$	8.085	−0.5481	23.87	25.32	25.(0.9)
		$-0.7365+1.273i$	$-3.434-2.875i$	$-0.3122-0.5250i$	−16.17	1.096			
	58	$0.3993-0.0910i$	$3.943+2.454i$	$0.2263+0.2829i$	6.590	−0.4079	13.23	13.65	14.14(0.33)
		$-0.1285+0.4016i$	$-2.168-1.815i$	$-0.1244-0.2092i$	−13.18	0.8158			
	50	$0.2367-0.0332i$	$2.930+1.824i$	$0.1250+0.1562i$	5.910	−0.3174	9.756	9.948	9.38(0.16)
		$-0.00269+0.1897i$	$-1.611-1.349i$	$-0.0687-0.1155i$	−11.82	0.6348			
150	92	$2.575-2.823i$	$7.662+5.048i$	$1.003+1.003i$	16.88	−1.643	55.51	59.89	58.(8.0)
		$-2.889+3.279i$	$-6.761-4.732i$	$-0.8850-0.9403i$	−19.49	1.898			
	82	$1.303-1.429i$	$6.087+4.010i$	$0.6330+0.6330i$	15.35	−1.460	39.25	41.62	40.1(1.9)
		$-1.399+1.736i$	$-5.371-3.760i$	$-0.5585-0.5934i$	−17.72	1.624			
	73	$0.7204-0.7196i$	$4.824+3.178i$	$0.3976+0.3976i$	14.00	−0.9493	30.07	31.37	31.6(2.0)
		$-0.6955+0.9101i$	$-4.257-2.980i$	$-0.3508-0.3727i$	−16.17	1.096			
	58	$0.2494-0.1934i$	$3.045+2.006i$	$0.1584+0.1584i$	11.41	−0.7065	17.25	17.64	
		$-0.1961+0.2644i$	$-2.687-1.881i$	$-0.1398-0.1485i$	−13.18	0.8158			
	50	$0.1329-0.0833i$	$2.263+1.491i$	$0.0875+0.0875i$	10.24	−0.5498	12.93	13.12	
		$-0.0901+0.1193i$	$-1.997-1.398i$	$-0.0772-0.0820i$	−11.82	0.6348			

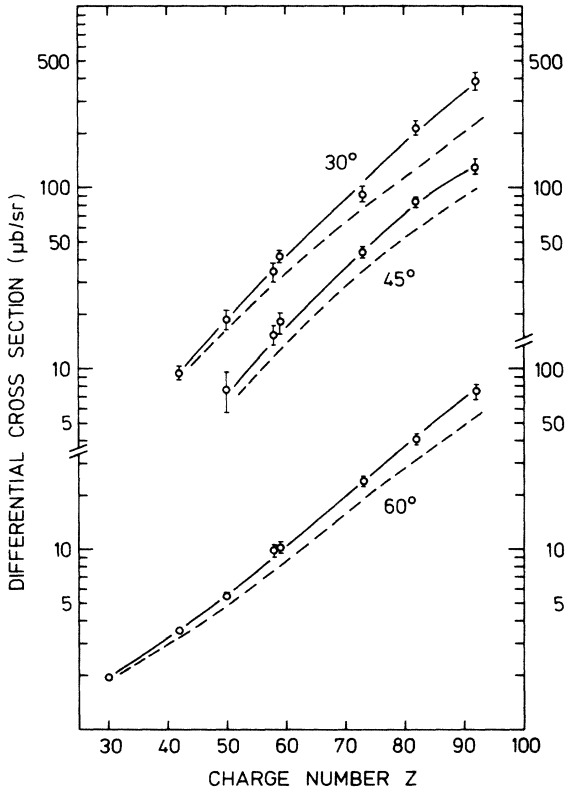

FIG. 4. Charge-number dependence of coherent elastic scattering for $E=2.754$ MeV and scattering angles of 30°, 45°, and 60°. Experiment compared with predictions. Dashed curves: including R, T, N, and lowest-order D scattering but not including the Coulomb correction term. Solid curves: same as dashed curves but including also the Coulomb correction term.

traction. The narrow peaks marked by arrows are due to elastic scattering, the broad peaks due to Compton scattering. The experimental data obtained at $\theta=15°$ and 7.7° are contained in Tables I–III and in Fig. 3. The experimental data for $\theta=30°$ and 45° are listed in Table IV and depicted in Figs. 4 and 5 together with elastic dif-

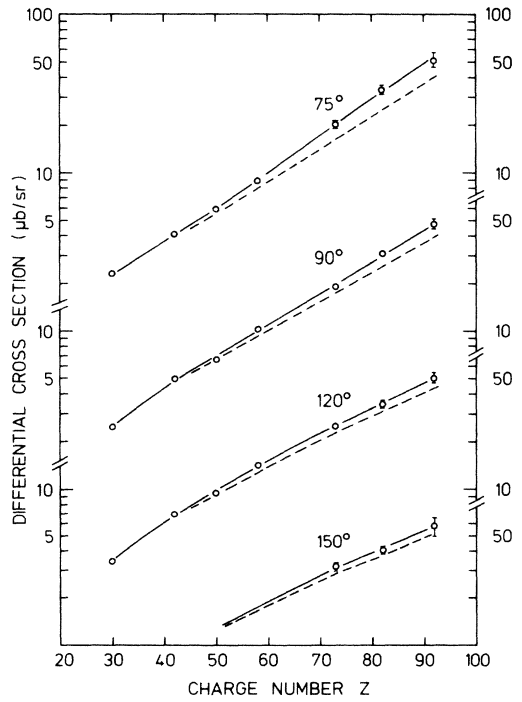

FIG. 5. Same as Fig. 4 but for scattering angles of 75°, 90°, 120°, and 150°.

ferential cross sections previously measured in the 60° to 150° angular range. From these previous studies[11] it was not completely clear whether or not there is a small contribution of nuclear resonance fluorescence (NRF) in the Ce data ($Z=58$). Therefore, in the present investigation elastic cross sections were measured also for a Pr ($Z=59$) scatterer. In Fig. 4 we see that all the data are nicely located at the same straight line, with the $Z=59$ slightly higher than the $Z=58$ data. We, therefore, have a good reason for the assumption that the $Z=58$ data do not contain contributions from NRF.

III. THEORY

We write the total coherent elastic scattering amplitude in the form

$$A=A^R+A^T+A^D+B^D+A^N \tag{1}$$

and the differential cross section either as

$$\frac{d\sigma}{d\Omega}=\tfrac{1}{2}(|A_{\parallel}|^2+|A_{\perp}|^2) \tag{2}$$

or in the form

$$\frac{d\sigma}{d\Omega}=(|A|^2+|A'|^2)\,. \tag{3}$$

In (2) and (3) $A_{\parallel}$ and $A_{\perp}$ are the amplitudes for scattering with linear polarization parallel and perpendicular to the scattering plane, respectively, and A and A' are the amplitudes for scattering without and with change of the state of circular polarization, respectively. The relations between the two sets of the scattering amplitudes are

$$\begin{aligned} A_{\parallel}&=A+A'\,,\\ A_{\perp}&=A-A'\,. \end{aligned} \tag{4}$$

We use the optical theorem in the form

$$\mathrm{Im}\,A(E,\theta=0)=\frac{E}{4\pi\hbar c}\sigma_{\mathrm{tot}}(E) \tag{5}$$

and the dispersion relation in the form

$$\mathrm{Re}\,A(E,\theta=0)=\mathrm{Re}\,A(E=0,\theta=0)+\frac{E^2}{2\pi^2\hbar c}\mathrm{P}\int_0^{\infty}\frac{\sigma_{\mathrm{tot}}(E')}{E'^2-E^2}dE'\,. \tag{6}$$

The use of (5) defines a sign convention, showing that imaginary parts of scattering amplitudes are positive at $\theta=0°$. In the case of the R amplitudes (6) has to be replaced by an expression defined relative to $\mathrm{Re}A(E=\infty,\theta=0)$ instead of $\mathrm{Re}A(E=0,\theta=0)$.[9]

Nuclear scattering. At the low energies of the present experiment finite-size effects of the nucleus are negligible. Therefore, we can simply use

$$A_{\perp}^N=\frac{E^2}{4\pi\hbar c}\mathrm{Re}\sum_{\nu=1}^{2}\sigma_\nu\Gamma_\nu\frac{E_\nu^2-E^2+iE\Gamma_\nu}{(E_\nu^2-E^2)^2+E^2\Gamma_\nu^2}\,, \tag{7}$$

$$A_{\perp}^T=-\frac{Z^2e^2}{Mc^2}\,, \tag{8}$$

$$A_{\parallel}^{N,T}=A_{\perp}^{N,T}\cos\theta\,, \tag{9}$$

for the amplitudes for nuclear Rayleigh (N) and nuclear Thomson scattering (T), respectively. In (7) E_ν, σ_ν, and

TABLE V. Comparison of different calculated real parts of L_I shell Rayleigh + nuclear Thomson amplitudes for $_{82}$Pb at 2.754 MeV in units of $10^{-3}\,r_0$.

	θ	S matrix[a]	RFF[b]	MRFF[c]	RFFR[d]	MRFFR[e]
	0	−1939	−2018	−1939	−1733	−1931
	1	−1665	−1742	−1665	−1494	−1658
	10	−62.85	−97.98	−65.70	−74.61	−63.93
	30	−18.84	−31.19	−21.01	−18.08	−18.41
$\mathrm{Re}A_{\parallel}$	60	−8.345	−10.45	−8.995	−8.26	−6.24
	90	−0.333	0.008	0.008	0.32	0.17
	120	9.131	9.25	8.89	9.11	9.05
	150	15.60	15.86	15.39	15.60	15.56
	180	17.97	18.26	17.76	17.97	17.94
	0	−1939	−2018	−1939	−1733	−1931
	1	−1666	−1742	−1666	−1494	−1658
	10	−64.42	−99.49	−66.71	−76.22	−65.29
	30	−23.01	−36.01	−24.27	−22.34	−22.90
$\mathrm{Re}A_{\perp}$	60	−18.08	−20.90	−18.00	−18.03	−18.75
	90	−18.01	−18.98	−17.76	−18.03	−17.92
	120	−17.99	−18.48	−17.75	−18.02	−17.96
	150	−17.99	−18.30	−17.76	−17.98	−17.95
	180	−17.97	−18.26	−17.76	−17.97	−17.94

[a]From second-order S matrix of QED.
[b]From relativistic form factor.
[c]From modified relativistic form factor.
[d]From K shell second-order S matrix and relativistic form factor ratio L_I/K.
[e]From K shell second-order S matrix and modified relativistic form factor ratio L_I/K.

TABLE VI. Imaginary parts of Rayleigh amplitudes for $_{82}$Pb at 2.754 MeV in units of 10^{-3} r_0 obtained from the second-order S matrix.

	Im $A_{\parallel}$			Im $A_{\perp}$		
θ	K shell	L shell	K/L	K shell	L shell	K/L
0	25.34	2.981	8.50	25.34	2.981	8.50
1	25.11	2.955	8.50	25.18	2.963	8.50
10	11.53	1.376	8.38	16.03	1.892	8.47
30	3.024	0:340	8.89	9.16	1.076	8.51
60	1.584	0.216	7.35	5.339	0.678	7.87
90	0.062	0.020	3.10	2.997	0.392	7.65
120	−0.775	−0.095	8.18	1.898	0.250	7.60
150	−1.176	−0.152	7.76	1.424	0.186	7.65
180	−1.293	−0.168	7.67	1.293	0.169	7.67

Γ_ν are the Lorentz parameters of the GDR.

Delbrück scattering. In (1) the amplitudes for D scattering are split up into the lowest-order term A^D and the Coulomb correction term B^D. The lowest-order terms A^D are known from calculations[6,11,15,16] based on the lowest-order Feynman graph. The Coulomb correction terms B^D will be evaluated from the experimental data in the next section.

Atomic Rayleigh scattering. In our previous investigation[11] on elastic scattering of 2.754 MeV photons only the K shell amplitudes had been calculated using the second-order S matrix of QED (SM). Contributions from higher shells were calculated via the relativistic modified form factor (MRFF).[17] Since only guesses were possible about the accuracy of this procedure, rather large uncertainties had to be assumed. Therefore, one of us (L.K.) has calculated the L_I amplitudes from the SM. Table V shows the results obtained for the real amplitudes of Pb together with predictions from different approximations. In agreement with the findings for the K shell, the MRFF is superior over the relativistic form factor (RFF). An even better approximation to the L_I shell SM amplitude is obtained by assuming that the ratios of amplitudes L_I/K are the same for the SM and the MRFF. Therefore, this assumption was applied to any other one of the higher shells whenever real parts of scattering amplitudes had to be calculated. For the sake of completeness it should be pointed out that Table V contains sums of T and L_I shell R amplitudes. This provides us with a realistic picture of the usefulness of the approximations, since T scattering is always part of the coherent elastic process. The L_I shell R amplitudes alone deviate drastically from the approximations when they are small.

Table VI shows a comparison of imaginary parts of SM scattering amplitudes for the K and L_I shells. It is apparent that the ratios K/L_I are almost independent of scattering angle. Since the zero-angle imaginary amplitudes are related to the photoabsorption cross sections via the optical theorem, use can be made of this K/L_I property to calculate precise imaginary parts of scattering amplitudes from the K shell SM amplitudes and the photoabsorption cross section of the subshell under consideration.

Table VII compares the present total atom R amplitudes with the ones used in previous high-precision investigations of D scattering.[11] The "true" errors of the previous amplitudes, being the differences between the previous and the present results, are one order of magnitude small-

TABLE VII. Comparison of previous (Ref. 11) with present improved total atom Rayleigh scattering amplitudes for Pb ($Z=82$) in units of 10^{-3} r_0. The photon energy is 2.754 MeV.

θ		Re $A_{\parallel}^R$	Im $A_{\parallel}^R$	Re $A_{\perp}^R$	Im $A_{\perp}^R$
60	a	4.76	1.94	−1.78	6.48
	b	4.78±0.80	1.90 ±0.32	−1.68±0.28	6.41 ±1.07
	c	+0.02	−0.04	−0.10	−0.07
90	a	2.41	0.088	−1.73	3.65
	b	2.36±0.39	0.08 ±0.01	−1.74±0.29	3.60 ±0.60
	c	−0.05	−0.008	+0.01	−0.05
120	a	1.54	−0.938	−1.60	2.31
	b	1.49±0.25	−0.93 ±0.15	−1.61±0.27	2.28 ±0.38
	c	−0.05	−0.008	+0.01	−0.03

[a]Present calculation with K and L_I shells from S matrix and other shells from relativistic modified for factor ratios.

[b]Previously used (Ref. 11) amplitudes with only the K shell from S matrix and adopted error.

[c]"True" error of previous calculation.

TABLE VIII. Total atom R amplitudes in units of $10^{-3}\ r_0$ calculated for $E=4.8$ MeV and $Z=92$.

θ	Re $A_{\parallel}^{SM}$	Re $A_{\parallel}^{MFF}$	Im $A_{\parallel}^{SM}$[a]	Re $A_{\perp}^{SM}$	Re $A_{\perp}^{MFF}$	Im $A_{\perp}^{SM}$[a]
15	−87.47	−111.5	3.297	−95.40	−115.44	11.38
30	0.3439	−5.423	2.261	−4.064	−6.262	7.886
45	0.6910	−0.018	0.7993	−2.186	−0.026	4.832
60	−0.2771	0.214	−0.1465	−2.376	0.429	3.053
75	−0.5190	0.095	−0.6645	−2.179	0.366	2.076
90	−0.4221	0.000	−0.9270	−1.814	0.279	1.550
105	−0.2026	−0.056	−1.047	−1.426	0.216	1.276
120	0.0258	−0.087	−1.089	−1.090	0.174	1.143
135	0.2173	−0.104	−1.092	−0.8162	0.148	1.087
150	0.3644	−0.114	−1.081	−0.6295	0.131	1.068

[a]Im $A_{\parallel}^{MFF} \equiv \mathrm{Im} A_{\perp}^{MFF} \equiv 0$.

er than the previously[11] quoted errors. This further corroborates the statements about D scattering as the test of vacuum polarization contained in our previous paper.[11]

In order to arrive at information about R scattering at higher energies, total atom R amplitudes were calculated for the whole angular range between $\theta=0°$ and 180°, for the energies between 3.2 and 4.8 MeV, and for charge numbers of $Z=82$ and 92. In these calculations the K shell amplitudes were obtained from the SM, whereas the higher-shell amplitudes were generated from the MRFF by the methods outlined above. As an example Table VIII shows the results obtained for $Z=92$ at 4.8 MeV. From this compilation we see that for scattering angles smaller than $\theta=30°$ the modified form factor is a useful estimate of the real part of the R scattering amplitude. Above this angle the modified form factor is only a qualitative estimate of the scattering amplitude. Therefore, the second-order S matrix provides an essential improvement although, as we shall see, detailed properties of R amplitudes do not necessarily show up in the elastic differential cross sections because of the contributions from other processes.

IV. RESULTS AND DISCUSSION

Results of the small-angle ($\theta=7.7°$ and 15°) measurements are discussed in Tables I–III and Fig. 3. Below 1 MeV the experimental differential cross sections are in agreement with all the three predictions, i.e., (1) MFF: including lowest-order D and R scattering as predicted by the modified form factor, (2) SM: including lowest-order D and R scattering generated by the SM procedures discussed in the preceding section, and (3) WD: not including D but including the SM predictions for R scattering. The agreement between theory and experiment is of the order of the experimental error, i.e., better than 3%. From this finding we have to conclude that, despite the shortcomings of the MFF discussed in the previous section, rather useful predictions are obtained from this approximation at small angles and energies below 1 MeV. Furthermore, as expected, D scattering does not contribute at these energies and these angles.

Above 1 MeV D scattering makes a contribution which increases strongly with energy. Indications for the Coulomb correction effect are visible above 2 MeV, increasing to a 70% deviation of the experiment from the lowest-order prediction (curves b in Fig. 3) at $E=3.253$ MeV and $Z=92$. A detailed discussion of the Coulomb correction effect at $\theta=15°$ is given in Table IX. We return to this after a more general discussion of the Coulomb correction effect carried out in the next paragraph.

The analysis of the Coulomb correction effect at 2.754

TABLE IX. Scattering amplitudes and differential cross sections for elastic scattering of 2.754 and 3.253 MeV photons from Pb and U through $\theta=15°$. The notations are the same as in Table IV.

E (MeV)	Z	$A_{R_\perp^\parallel}$ ($10^{-3}\ r_0$)	$A_{D_\perp^\parallel}$ ($10^{-3}\ r_0$)	$B_{D_\perp^\parallel}$ ($10^{-3}\ r_0$)	$A_{T_\perp^\parallel}$ ($10^{-3}\ r_0$)	$A_{N_\perp^\parallel}$ ($10^{-3}\ r_0$)	$d\sigma/d\Omega_{LO}$ (mb/sr)	$d\sigma/d\Omega$ (mb/sr)	$d\sigma/d\Omega_{expt}$ (mb/sr)
	92	$-409.8+11.45i$	$171.3+87.89i$	$-34.03+37.25i$	-18.83	1.833	7.401	9.438	10.00(2.00)
		$-433.8+24.11i$	$130.7+67.60i$	$-26.46+29.57i$	-19.49	1.898			
2.754									
	82	$-319.8+7.016i$	$136.1+69.82i$	$-21.48+23.51i$	-17.12	1.569	4.514	5.364	4.700(0.700)
		$-339.5+14.63i$	$103.8+53.71i$	$-16.70+18.67i$	-17.72	1.624			
	92	$-289.3+7.372i$	$193.5+128.0i$	$-60.89+37.97i$	-18.83	2.460	3.015	5.180	5.450(0.400)
		$-307.1+18.81i$	$144.2+93.81i$	$-45.38+27.83i$	-19.49	2.547			
3.253									
	82	$-212.9+4.779i$	$153.7+101.7i$	$-38.43+23.96i$	-17.12	2.281	1.604	2.566	2.486(0.377)
		$-226.1+11.61i$	$114.5+74.53i$	$-28.64+17.56i$	-17.72	2.361			

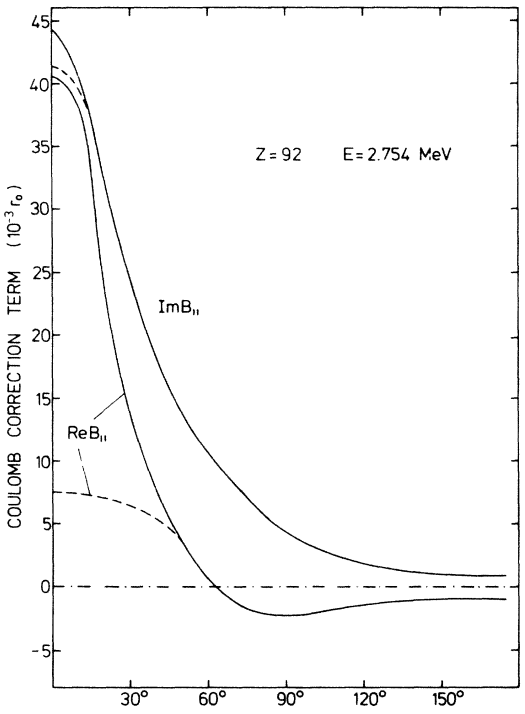

FIG. 6. Coulomb correction terms for scattering with the plane of polarization parallel to the scattering plane. Solid curve: extrapolated to the predicted zero-angle result not including the screening correction. Dashed curve: same as solid curve but taking into account the screening correction.

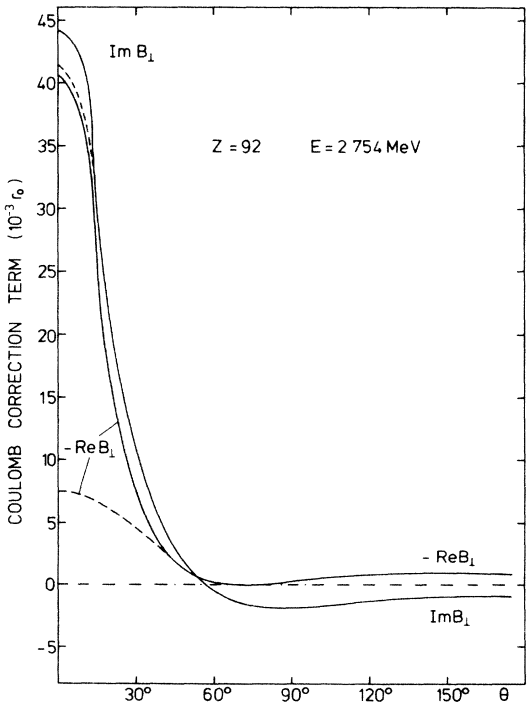

FIG. 7. Same as Fig. 6 but with the plane of polarization perpendicular to the scattering plane.

MeV is carried out in Table IV and Figs. 4–7. The Coulomb correction terms presented have been generated using the following arguments.

(i) At $\theta=0°$ the Coulomb correction terms are known via optical theorem and dispersion relation from the pair production cross section.[13,14] Since the amplitude A' for scattering with change of the state of circular polarization vanishes at $\theta=0°$, the amplitudes for linear polarization parallel and perpendicular to the scattering plane must be equal to each other and must have the same signs, i.e., $B_{||}^{D}=B_{\perp}^{D}$.

(ii) At $\theta=180°$ we have $A=0$ and therefore $B_{||}^{D}=-B_{\perp}^{D}$.

(iii) As known from previous experiments,[10,11] Coulomb correction increases the differential cross section at large angles in this energy domain. Therefore, at large angles where the leading terms $\mathrm{Re}A^{D}$ and A^{T} have the same signs both for the parallel and perpendicular components, $\mathrm{Re}B_{||}^{D}$ and $\mathrm{Re}B_{\perp}^{D}$ should also have the same signs as $\mathrm{Re}A_{||}^{D}$ and $\mathrm{Re}A_{\perp}^{D}$, respectively.

(iv) The last supposition used in the analysis, i.e., that at $\theta=180°$ the relations $\mathrm{Re}B_{||}^{D}=\mathrm{Im}B_{||}^{D}$ and $\mathrm{Re}B_{\perp}^{D}=\mathrm{Im}B_{\perp}^{D}$ should be valid, might appear arbitrary at first sight. However, there is some justification for this because of the fact that the same relations approximately hold for the lowest-order amplitudes.

Using (i)–(iv) as guidelines, a smooth curve was fitted to the experimental data, by varying the four Coulomb correction amplitudes $\mathrm{Re}B_{||}$, $\mathrm{Im}B_{||}$, $\mathrm{Re}B_{\perp}$, and $\mathrm{Im}B_{\perp}$ in a way that the ratios of the parallel and perpendicular amplitudes were the same for the Coulomb correction and lowest-order amplitudes.

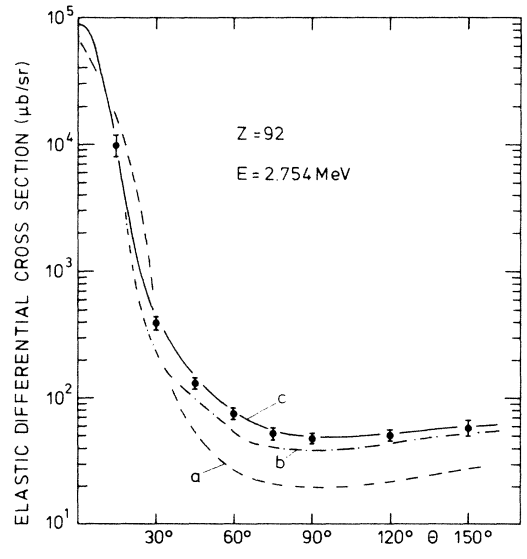

FIG. 8. Experimental coherent elastic scattering cross sections for $Z=92$ and $E=2.754$ MeV compared with different predictions: (a) including only R, N, and T scattering, (b) including R, T, N, and lowest-order D scattering, but not including the Coulomb correction effect, (c) same as (b) but including also the Coulomb correction effect.

As a conclusion, we are confident that within a margin of arbitrariness the curves in Figs. 6 and 7 should resemble the Coulomb correction terms at $E=2.754$ MeV. Furthermore, the proportionality of the Coulomb correction terms with $\alpha(Z\alpha)^4$ previously observed at large angles, is found to be valid also for $\theta=30°$ and 45° (Figs. 4 and 5).

Zero-angle Coulomb correction terms have been calculated without and with including also a screening correction.[14] These zero-angle results and their extrapolation to larger angles are shown in Figs. 6 and 7. It was of interest to us to see whether or not effects of screening are visible also in the experimental data. For this purpose we have replaced the solid curve of Fig. 8, which does not include screening, by a curve also including the screening correction. The shift of the prediction obtained in this way was at most 10% and therefore not visible in the figure.

We now return to Fig. 3. There is reasonable evidence for a Coulomb correction effect at $\theta=15°$ and energies above 2.5 MeV which we have analyzed by the same procedure as described above for the 30° to 150° angular range. The results are listed in Table IX.

V. CONCLUSIONS

A systematic investigation of elastic photon scattering in the 0°–150° angular range and 1–4 MeV energy range has led to valuable information about atomic Rayleigh (R) and Delbrück (D) scattering. The relativistic modified form factor (MRFF), though only partly justified by the second-order S matrix (SM), proved to be an appropriate basis for the prediction of R scattering.

Coulomb correction terms for D scattering are of the order of $\alpha(Z\alpha)^4$ with no indication of higher orders in Z in the whole angular range between 15° and 150°. Tentative estimates of the Coulomb correction terms are generated between 0° and 180° on the basis of partly firm, partly tentative arguments. Large modifications of the real parts of the Coulomb correction terms due to screening as predicted by the dispersion relation do not show up in the experimental data because they are masked by other coherent elastic processes.

This work was supported by Deutsche Forschungsgemeinschaft through contract Schu 222.

---

*Present address: IBM Deutschland GmbH, 7032 Sindelfingen, Federal Republic of Germany.

[1]M. Schumacher, F. Smend, P. Rullhusen, and W. Mückenheim, in Neutron-Capture Gamma-Ray Spectroscopy and Related Topics, 1981, edited by T. v. Egidy, F. Gönnenwein, and B. Maier, Inst. of Phys. Conf. Ser. **62**, 598 (1982).

[2]R. Moreh, in *Intermediate Energy Nuclear Physics,* edited by R. Bergère, S. Costa, and C. Schaerf (World-Scientific, Singapore, 1982), p. 1.

[3]M. Schumacher, in *Capture Gamma-Ray Spectroscopy and Related Topics—1984,* Proceedings of the Fifth International Symposium on Capture Gamma-Ray Spectroscopy and Related Topics, AIP Conf. Proc. No. 125, edited by S. Raman (AIP, New York, 1984), p. 166.

[4]L. Kissel and R. H. Pratt, Phys. Rev. Lett. **40**, 387 (1978).

[5]L. Kissel, R. H. Pratt, and S. C. Roy, Phys. Rev. A **22**, 1970 (1980).

[6]P. Papatzacos and K. Mork, Phys. Rep. **21C**, 81 (1975).

[7]W. Mückenheim and M. Schumacher, J. Phys. G **6**, 1237 (1980).

[8]L. Kissel, S. C. Roy, and R. H. Pratt, in *X-Ray and Atomic Inner-Shell Physics—1982* (University of Oregon), Proceedings of the International Conference on X-Ray and Atomic Inner-Shell Physics, AIP Conf. Proc. No. 94, edited by B. Crasemann (AIP, New York, 1982).

[9]L. Kissel and R. H. Pratt, in *Atomic Inner-Shell Physics,* edited by B. Crasemann (Plenum, New York, 1985).

[10]P. Rullhusen, F. Smend, M. Schumacher, A. Hanser, and H. Rebel, Z. Phys. A **293**, 287 (1979).

[11]P. Rullhusen, W. Mückenheim, F. Smend, M. Schumacher, G. P. A. Berg, K. Mork, and L. Kissel, Phys. Rev. C **23**, 1375 (1981).

[12]P. Rullhusen, U. Zurmühl, F. Smend, M. Schumacher, H. G. Börner, and S. A. Kerr, Phys. Rev. C **27**, 559 (1983).

[13]F. Rohrlich, Phys. Rev. **108**, 169 (1957).

[14]R. Solberg, K. Mork, and I. Øverbø, private communication.

[15]P. Papatzacos and K. Mork, Phys. Rev. D **12**, 206 (1975); and private communication.

[16]T. Bar-Noy and S. Kahane, Nucl. Phys. **A288**, 132 (1977).

[17]D. Schaupp, M. Schumacher, F. Smend, P. Rullhusen, and J. H. Hubbell, J. Phys. Chem. Ref. Data **12**, 467 (1983).

[18]W. Mückenheim, P. Rullhusen, F. Smend, and M. Schumacher, Z. Phys. **300**, 43 (1981).